Volume 1 | Number 1 | Jan 2013 | Pages 1–100

Journal of
Materials Chemistry C

Materials for optical and electronic devices
www.rsc.org/materialsC

ROYAL SOCIETY
OF CHEMISTRY

ROYAL SOCIETY
OF CHEMISTRY

www.rsc.org/materialsC

Journal Name

COMMUNICATION

Patterning rubrene crystalline thin film for sub-micrometer channel length field-effect transistor arrays

Juan Zhu,[‡][a] Wenchong Wang,[‡][a] Qigang Zhong,[b] Liqiang Li,[a] Chuan Du,[a] Aifeng Lv,[a] Hong Wang,[a] Harald Fuchs,[a] and Lifeng Chi*[ab]

In the communication, a direct coupling of patterned growth of rubrene crystalline thin film with OFET fabrication is presented. The film was grown between pre-patterned Au electrodes covered with an organic monolayer, which directly allowed the fabrication of OFET devices with a sub-micrometer channel length. More importantly, closed packed and porous film structures can be controlled by adjusting the space of the electrodes, resulting in a two order difference in carrier mobility. The technique is completely compatible with lithography methods thus may find potential applications in addressable and crosstalk suppressing OFET arrays.

Introduction

Organic field-effect transistors (OFETs) have attracted increasing attention owing to their promising applications in

[a] J. Zhu, ‡ Dr. W. C. Wang, ‡ Dr. L. Q. Li, Dr. C. Du, Dr. A. Lv, H. Wang, Prof. H. Fuchs, Prof. L. F. Chi.

Physikalisches Institut and Center for Nanotechnology (CeNTech) Universität Münster, 48149 Münster, Germany

E-mail: chi@uni-muenster.de, chilf@suda.edu.cn

[b] Q. G. Zhong, Prof. L. F. Chi, Institute of Functional Nano & Soft Materials (FUNSOM) and Jiangsu Key Laboratory for Carbon-based Functional Materials & Devices Soochow University, Suzhou 215123, P. R. China

‡ These authors contributed equally to this work.

low-cost and flexible electronics.[1-3] However, one of the main issues for the further success of OFETs is the achievement of higher operating frequency, which is a key parameter for the radio frequency (RF) devices and circuits.[4] Generally speaking, the operating frequency is determined by both carrier mobility of the organic films and channel length of the devices.[5] A number of works have been dedicated to improve the carrier mobility via either synthesis of molecules with strong inter-molecule coupling and/or growth of high quality crystalline films.[6-7] In comparison, less attention is paid to decrease the channel length of the devices owing to absence of suitable patterning techniques.[8-12] As organic materials are chemically and mechanically fragile, which tend to be easily damaged at high temperature, in solvents and under energetic particles, conventional mature patterning techniques for inorganic materials based on photolithography and etching can thus not be simply applied to organic materials.[13-15] Therefore, coupling of material growth with device fabrication, with uniform crystalline film over large area and precise position control with high resolution, still remains a big challenge.

Among small molecular organic semiconductors, rubrene ($C_{42}H_{28}$: 5, 6, 11, 12-tetraphenylnaphthacene, chemical structure shown in **Figure 1a**) has received great interests owing to its high carrier mobility.[16,17] Initial works on rubrene single bulk crystal demonstrated a hole mobility up to 15-20 cm^2/V•s.[18] However, challenge in growing of high quality rubrene crystalline thin films sets an obstacle in their electronic applications.[19,20] Many efforts have been given for producing crystalline rubrene thin film over dielectric layers toward large area electronics, including "hot-wall" deposition, in-situ vacuum annealing, solution-processing technique and abrupt heating technique.[21-23] Although the techniques have been successfully applied to the fabrication of OFETs, they suffer from either rigorous experiment environments and/or lower charge mobility of 0.01-0.1 cm^2/V•s.[24,25]

Recently, strategy of template induced crystallization was proposed to produce high quality rubrene crystalline films.[26,27] In 2010, Xu's group reported a new strategy of using flat thin layers of 6,13-pentacenequinone (PQ) as a template to induce the crystallization of rubrene in vacuum-deposited thin amorphous films.[28] More recently, we demonstrated the converting of amorphous rubrene micro-islands to high quality porous crystalline thin films on a monolayer of phospholipid, DPPC (1, 2-dipalmitoyl-sn-glycero-3-phosphocholine, **Figure 1b**), covered SiO$_2$.[29] However, in our previous work we could not link the film growth and device fabrication directly together, especially the fabrication for integrated and addressable circuits. In this study, we extend our previous work and demonstrate the direct fabrication of rubrene crystalline thin film on DPPC covered SiO$_2$ surfaces between Au patterns, yielding a sub-micrometer channel length bottom-contact OFETs with a hole mobility up to 0.16 cm^2/V•s. More interestingly, the morphology of the thin films can be controlled simply by adjusting with the pre-defined Au electrodes' gaps, resulting in a two order of magnitude difference in hole mobility. The proof of principle for the fabrication of addressable OFET arrays is provided as well. The process is completely compatible with lithography methods, particularly cost effective nanoimprint lithography, and can be used to fabricate large area and addressable OFET arrays with suppressed cross-talk between adjacent devices.

Results and discussion
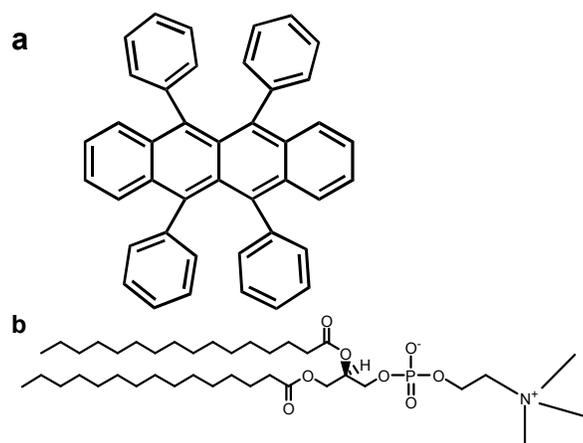
Figure 1. Chemical structure of (a) rubrene, and (b) DPPC.

The schematic representation for the fabrication process of the patterned crystalline rubrene film is depicted in **Figure 2(a-f)**. Firstly, Au patterns on SiO$_2$ surface were created by Electron Beam Lithography (EBL) technique, shown in **Figure 2a**. Then the templates were either covered by a DPPC monolayer transferred via LB method (**Figure 2d**) or used directly as reference samples. Both types of samples were loaded into a vacuum chamber to deposit rubrene molecules at room
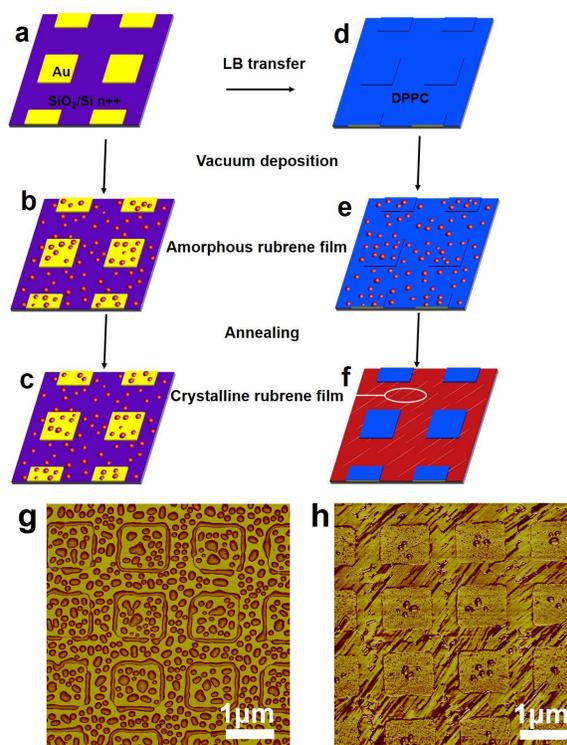
Figure 2. (a-f) A schematic illustration of topographical evolution of rubrene deposited onto SiO$_2$ surface pre-patterned with Au-structures without (a-c) and with DPPC monolayer coverage (d-f). (g, h) AFM phase images of rubrene on Au-template surface without (g) and with DPPC monolayer (h) annealed at 80 ºC for 8 hours in a high vacuum (~10^{-8} mbar).

temperature. After deposition, the samples were taken out from vacuum chamber for Atomic Force Microscope (AFM) measurements. The as-grown samples showed similar morphologies on both templated surfaces, with dome-like islands randomly distributed as illustrated in **Figure 2b** and **2e**, which are consistent with the amorphous nature of these films.[30a] After AFM inspection, the samples were loaded into the vacuum chamber for annealing. No obvious morphology changes were observed for samples of Au patterned SiO$_2$ surfaces (**Figure 2e**). However with DPPC monolayer coverage, the rubrene film exhibited a significant morphology transition from dome-like islands to orientated film between Au patterns (**Figure 2f**). Figure 2g depicts an AFM image of rubrene amorphous structures on Au patterned SiO$_2$ surface after annealing. In comparison with the morphology that before annealing (see supporting information **S2**), the amorphous rubrene islands become more non-uniform and higher, because rubrene molecules can dismantle from smaller islands and diffuse into big ones during the annealing process. In contrast, the morphology on DPPC monolayer covered Au pre-template underwent a transition from dome shaped islands to well close packed, orientated rubrene crystalline thin film (**Figure 2h**). Certain alignment can be observed in **Figure 2h**. We believe the orientation is relative to the step edges of the pre-patterns,

which is similar to the alignment of crystal on the atomic step.[30b] We also did experiments at different annealing time. Between 0 - 6 h, amorphous rubrene remain dome-shaped islands on the surface. The crystallization takes place in the last two hours. The mechanism of the crystallization and solutions to shorten annealing time are still under investigation.
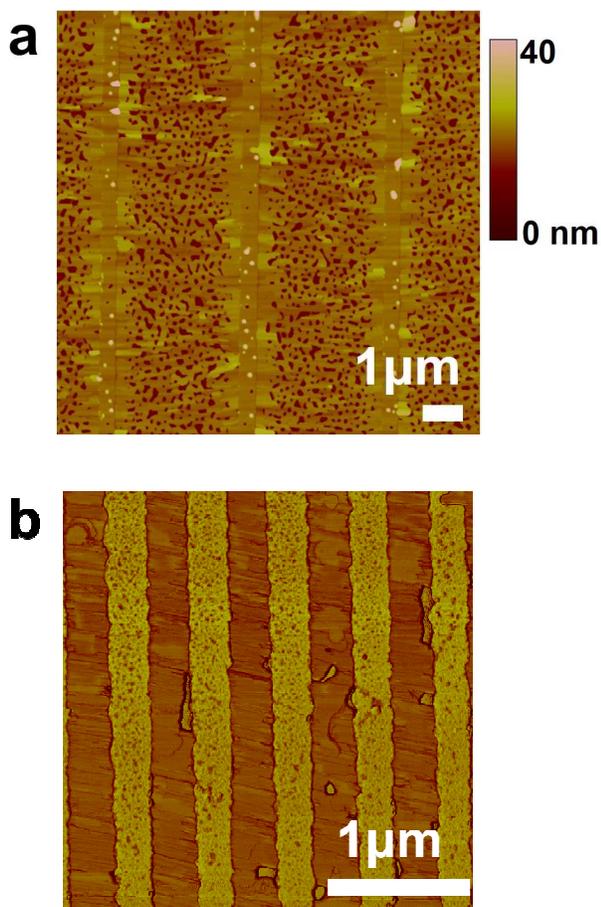
Figure 3. AFM images of rubrene on DPPC monolayer covered SiO_2 surface, pre-templated with 0.25 μm Au line with different spacing (a) 3 μm and (topography image) (b) 0.3 μm (phase image). The samples were annealed at 80 ºC for 8 hours in a high vacuum (~10^{-8} mbar).

It is notable that this method can be extended to different template structures. **Figure 3** shows AFM images of rubrene on SiO_2 surface, which are patterned Au lines with 0.25 μm in width. The Au lines, shown in **Figure 3a** and **3b**, are spaced in 0.3 μm and 3 μm respectively. The surfaces were covered with the DPPC monolayer, and the samples were annealed at 80 ºC for 8 hours after deposition of rubrene molecules, as described previously. As illustrated in **Figure 3a**, for Au lines spaced in 3 μm, close packed rubrene crystalline film is observed in the region near Au lines. However, the film becomes porous with irregular holes in middle region between Au lines, similar to rubrene on DPPC covered SiO_2 substrates as we observed in an earlier work [29]. The porous structure originates during the

annealing process as described previously.[29] The close packed rubrene film in the region near Au lines is about 0.2 μm in width, which might be caused by the migration of molecules from Au surface to the edges areas which provide preferential sites for nucleation.[31,32] The diffusion limited crystallization enables us to grow close packed rubrene directly between Au stripes by reducing the channel length. **Figure 3b** depicts an AFM image of the close packed rubrene film between the Au lines with a space in 0.3 μm.
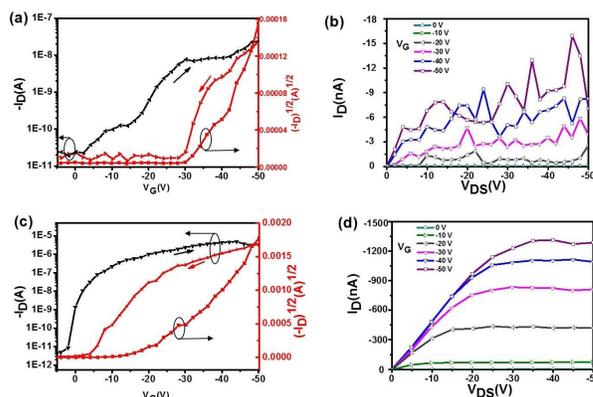
Figure 4. Electrical characteristics for rubrene OFETs on liquid-condensed (LC) DPPC/Au template SiO_2 substrates with Au-line spaced in (a, b) 3 μm and (c, d) 0.3 μm. (a, c) Drain current (I_D) and square root of the drain current versus gate voltage (V_G) curves scanned in the forward (black line) and reverse (red line) direction at a drain-source voltage of -40 V. (b, d) Drain current versus drain voltage characteristics for various gate voltages (V_D) corresponding to the transfer characteristics of (a, c) respectively.

We further measured the field effect electrical properties of the both porous and close packed rubrene crystalline films as shown in **Figure 3a and 3b**. The devices were prepared on highly doped Si with 300 nm thermal oxide by taking the Si as the gate electrode, the Au pattern as the source and drain electrodes. **Figure 4a** discloses the transfer characteristic of OFET with porous structure, yielding a hole mobility in the saturation region of 0.002 cm^2/V•s. In contrast, shown in **Figure 4c**, in the transfer characteristics of OFETs with the close packed structure, the source-drain current is almost two order larger than that with porous structure giving the hole mobility of 0.16 cm^2/V•s and the on-off ratio of 10^5. The relatively poor mobility in 3 μm channel length OFETs can be attributed to the porous structure which is consisted of crystalline grains connected to each other. In this case, the porous structure contains many grain boundaries that serve as energy barrier for electron transfer. In contrast, with in 0.3 μm channel length the OFETs confirm the high quality of the rubrene films. Here we have taken the bottom contact into consideration: the mobility measurement by bottom contact OFETs are normally one order lower than that by top contact.[33,2] Furthermore, we expect a high operating frequency fc of the devices according to fc $\propto$ μ/L^2 (where μ is carrier

mobility and L is the channel length of the devices),[5,34] which will be conducted in later experiments. We observe much larger hysteresis and SNR (Signal to Noise Ratio) in the OFETs with the porous rubrene structure shown in **Figure 4a** and **4b**, compared with the OFETs with the close packed rubrene structure shown in **Figure 4c** and **4d**. The relatively inferior field-effect behavior in 3 μm channel length could originate from hole-trapping density possibly induced by much more grain boundaries in porous structures.[35]
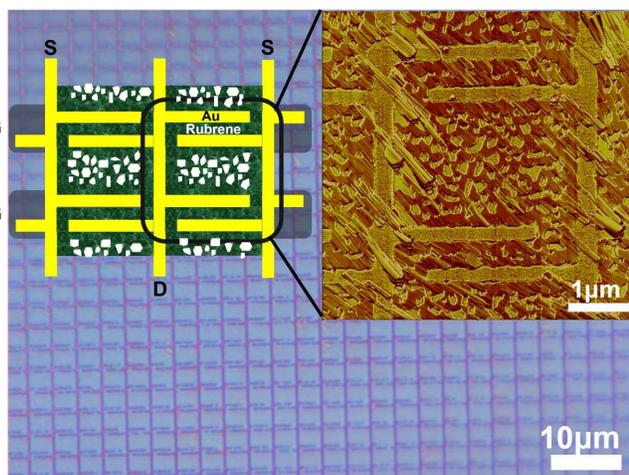
Figure 5. The optical image of large area, addressable OFET array. Insert: a schematic illustration of device configuration and surface morphology viewed by AFM phase image.

Lastly we present the versatility of the technique for fabricating large area OFET arrays for integration, as shown in **Figure 5**. Each pixel of the array represents an OFET with channel length of 0.3 μm, width of 0.25 μm and total length of 2.5 μm, as schematically depicted in the insert of **Figure 5**. The pixel is repeated along row and column directions in 3 μm. The pixel can be independently addressed via applying voltage on gate and source electrodes. One key challenge for OFET circuit is the crosstalk issue, as the device dimensions going down to sub-micrometer. The crosstalk is defined as mis-turn on the adjacent devices during the operating. Patterning active layer of FETs has been proved as an efficient way to minimize the crosstalk effect.[36] In our case, different structures of rubrene thin films, with alternating close packed crystals in channels and porous grain between pixels shown in insert of AFM image (phase image) in **Figure 5**, are demonstrated. The structures lead to 0.16 cm^2/V•s in the channels and 0.002 cm^2/V•s between the pixels, as demonstrated in **Figure 4**. The two orders difference in mobility can be utilized to design organic RF devices and circuits for high performance.

Conclusions

In summary, we present a simple but effective method to couple the growth of crystalline rubrene films and OFETs fabrication. The method is achieved by annealing of amorphous rubrene films on DPPC monolayer covered SiO$_2$ surfaces with pre-patterned Au electrodes. More importantly, closed packed and porous film structures can be controlled by adjusting the space between the electrodes, resulting in a two-order difference in carrier mobility in the films. The principle setup of addressable OFET array with channel length down to 0.3 μm is demonstrated. In addition, the technique we demonstrated here is completely compatible with lithography methods for scaling up.

Experimental

All the patterns were generated by e-beam lithography (EBL) (an Elphy 100 system attached to a LEO 1530 VP Gemini electron microscope) on heavily doped Si (100) with a 300 nm thermal oxide. A PMMA layer was first spin-coated on SiO$_2$/Si substrate with a thickness of 100 nm. After EBL, the substrates were developed and loaded into a vacuum chamber to coat 4 nm Cr adhesion layer and 30 nm Au layer by thermal evaporation. After a sequential ultrasonic lift-off process (submerging into acetone for 60 minutes) and cleaning in chloroform, acetone, ethanol, and de-ionized water, the pre-patterned substrates were O$_2$-plasma treated at 1 mbar and 300 watts for 2 minutes. Then a DPPC (purchased from Aldrich, 99%) monolayer was transferred using Langmuir-Blodgett (LB) technique at a high surface pressure of 40 mN/m with a low transfer velocity of 5 mm/min onto the pre-patterned SiO$_2$ substrates. The concentration of DPPC in chloroform was 1mg/ml. The subphase-thermostat was kept at 26.8 ℃. The room temperature was kept at 22 ℃ and humidity was constant at about 40%. LC DPPC/pre-patterned SiO$_2$ substrates were introduced into a high vacuum (~10^{-8} mbar) and degassed. Rubrene (purchased from Fluka Analytical, 95.0% (UV)) molecules were sublimed from a quartz crucible and deposited on the substrate at a deposition rate of 1 nm/min. Subsequently the samples were in-situ thermally annealed at 80 ℃ for 8 h. Then as-grown samples were analysed ex by AFM (Digital Instrument nanoprobe atomic force microscope 3000 in tapping mode) and Optical microscope (Olympus optical microscope equipped with CDD under bright field mode). The electrical characteristics of the OFETs were measured using a Keithley 4200 semiconductor parameter analyser under ambient conditions in a dark environment.

Acknowledgements

Notes and references

† Footnotes should appear here. These might include comments relevant to but not central to the matter under discussion, limited experimental and spectral data, and crystallographic data.

Electronic Supplementary Information (ESI) available: [details of any supplementary information available should be included here]. See DOI: 10.1039/c000000x/

References

1 H. Klauk, *Chem. Soc. Rev.*, 2010, **39**, 2643.

2 C. D. Dimitrakopoulos and P. R. L. Malenfant, *Adv. Mater.*, 2002, **14**, 99.

3 H. Dong, X. Fu, J. Liu, Z. Wang and W. Hu, *Adv. Mater.*, 2013, **25**, 6158.

4 Y.-M. Lin, K. A. Jenkins, A. Valdes-Garcia, J. P. Small, D. B. Farmer and P. Avouris, *Nano Lett.*, 2008, **9**, 422.

5 J. N. Haddock, X. H. Zhang, S. J. Zheng, Q. Zhang, S. R. Marder and B. Kippelen, *Org. Electr.*, 2006, **7**, 45.

6 S. C. B. Mannsfeld, J. Locklin, C.Reese, M. E. Roberts, A. J. Lovinger and Z. N. Bao, *Adv. Funct. Mater.*, 2007, **17**, 1617.

7 N. Stingelin-Stutzmann, E. Smits, H. Wondergem, C. Tanase, P. Blom, P. Smith and D. Deleeuw, *Nature Mater.*, 2005, **4**, 601.

8 C. Reese and Z. N. Bao, *Adv. Funct. Mater.*, 2009, **19**, 763.

9 S. G. Bucella, G. Nava, K. C. Vishunubhatla and M. Caironi, *Org. Electr.*, 2013, **14**, 2249.

10 H. Kang, R. Kitsomboonloha, J. Jang and V. Subramanian, *Adv. Mater.*, 2012, **24**, 3065.

11 F. Ante, D. Käblein, U. Zschieschang, T. W. Canzler, A. Werner, K. Takimiya, M. Ikeda, T. Sekitani, T. Someya and H. Klauk, *Small*, 2011, **7**, 1186.

12 K. Tukagoshi, F. Fujimori, T. Minari, T. Miyadera, T. Hamano and Y. Aoyagi, *Appl. Phys. Lett.*, 2007, **91**, 113508.

13 E. Menad, M. A. Meitl, Y. Sun, J.-U. Park, D. J.-L. Shir, Y.-S. Nam, S. Jeon and J. A. Rogers, *Chem. Rev.*, 2007, **107**, 1117.

14 D. Braga and G. Horowitz, *Adv. Mater.*, 2009, **21**, 1473.

15 D. J. Gundlach, T. N. Jackson, D. G. Schlom and S. F. Nelson, *Appl. Phys. Lett.*, 1999, **74**, 3302.

16 (a) V. Podzorov, S. E. Sysoev, E. Loginova, V. M. Pudalov and M. E. Gershenson, *Appl. Phys. Lett.*, 2003, **83**, 3504; (b) V. C. Sundar, J. Zaumseil, V. Podzorov, E. Menard, R. L. Willett, T. Someya, M. E. Gershenson and J. A. Rogers, *Science*, 2004, **303**, 1644.

17 V. Podzorov, E. Menard, A. Borissov, V. Kiryukhin, J. A. Rogers and M. E. Gershenson, *Phys. Rev. Lett.*, 2004, **93**, 086602.

18 V. Podzorov, *MRS Bulletin*, 2013, **38**, 15.

19 S. Seo, B.-N. Park and P. G. Evans, *Appl. Phys. Lett.*, 2006, **88**, 232114.

20 C. H. Hsu, J. Deng, C. R. Staddon and P. H. Beton, *Appl. Phys. Lett.*, 2007, **91**, 193505.

21 Y. Chen and I Shih, *Appl. Phys. Lett.*, 2009, **94**, 083304.

22 S.-W. Park, S. H. Jeong, J.-M. Choi, J. M. Hwang, J.H. Kim and S. Im, *Appl. Phys. Lett.*, 2007, **91**, 033506.

23 H. M. Lee, H. Moon, H.-S. Kim, Y. N. Kim, S.-M. Choi, S. Yoo and S. O. Cho, *Org. Electr.*, 2011, **12**, 1446.

24 S.-W. Park, J. M. Hwang, J.-M. Choi, D. K. Hwang, M. S. Oh, J. H. Kim and S. Im, *Appl. Phys. Lett.*, 2007, **90**, 153512.

25 H. M. Lee, J. J. Kim, J. H. Choi, S. O. Cho, *ACS NANO*, 2011, **5**, 8352.

26 W.-S. Hu , S.-Z. Weng , Y.-T. Tao , H.-J. Liu and H.-Y. Lee, *Org. Electr.*, 2008, **9**, 385.

27 J. H. Seo, D. S. Park, S. W. Cho, C. Y. Kim, W. C. Jang, C. N. Whang and K.-H. Yoo, *Appl. Phys. Lett.*, 2006, **89**, 163505.

28 Z. F. Li, J. Du, Q. Tang, F. Wang, J.-B. Xu, J. C. Yu and Q. Miao, *Adv. Mater.*, 2010, **22**, 3242.

29 C. Du, W. C. Wang, L. Q. Li, H. Fuchs and L. F. Chi, *Org. Electr.*, 2013, **14**, 2534.

30 (a) Y. Luo, M. Brun, P. Rannou and B. Grevin, *Phys. Stat. Sol. (a)*, 2007, **204**, 1851; (b) V. Ignatescu and J.-C. M. Hsu, *Appl. Phys. Lett.*, 2006, **89**, 253116.

31 (a) D.J. Gundlach,J. E. Royer, S. K. Park, S. Subramanian, O. D. Jurchescu, B. H. Hamadani, A. J. Moad, R. J. Kline, L. C. Teague, O. Kirillov, C. A. Richter, J. G. Kushmerick, L. J. Richter, S. R. Parkin, T. N. Jackson and J. E. Anthony, *Nature Mater.*, 2008, **7**, 216; (b) W. C. Wang, C. Du, D. Y. Zhong, M. Hirtz, Y. Wang, N. Lu, L. X. Wu, D. Ebeling, L.Q. Li, H. Fuchs and L.F. Chi, *Adv. Mater.*, 2009, **21**, 4721.

32 D. G. Oteyza, E. Barrena, M. Ruiz-Ose´s, I. Silanes, B. P. Doyle, J. E. Ortega, A. Arnau, H. Dosch and Y. Wakayama, *J. Phys. Chem. C*, 2008, **112**, 7168.

33 (a) K. Kim, M. K. Kim, H. S. Kang, M. Y. Cho, J. Joo, J. H. Kim, K. H. Kim, C. S. Hong and D. H. Choi, *Synthetic Metals*, 2007, **157**, 481; (b) A. R. Murphy and J. M. J. Fre´chet, *Chem. Rev.*, 2007, **107**, 1066.

34 M. Uno, T. Uemura, Y. Kanaoka, Z. H. Chen, A. Facchetti and J. Takeya, *Org. Electr.*, 2013, **14**, 1656.

35 (a) M. Egginger, S. Bauer, R. Schwödiauer, H. Neugebauer and N. S. Sariciftci, *Monatsh Chem*, 2009, **140**, 735; (b) M. Egginger, M. Irimia-Vladu, R. Schwödiauer, A. Tanda, T. Frischauf, S. Bauer and N. S. Sariciftci, *Adv. Mater.*, 2008, **20**, 1018.

36 A. L. Briseno, S. C. B. Mannsfeld, M. M. Ling, S. H. Liu, R. J. Tseng, C. Reese, M. E. Roberts, Y. Yang, F. Wudl and Z. N. Bao, *Nature*, 2006, **444**, 913.